analytical chemistry

pubs.acs.org/ac Article

Improved Dynamic Range, Resolving Power, and Sensitivity Achievable with FT-ICR Mass Spectrometry at 21 T Reveals the Hidden Complexity of Natural Organic Matter

William Bahureksa, Thomas Borch,* Robert B. Young, Chad. R. Weisbrod, Greg T. Blakney, and Amy M. McKenna*

Cite This: *Anal. Chem.* 2022, 94, 11382−11389 Read Online

ACCESS | Metrics & More | Article Recommendations | Supporting Information

ABSTRACT: Fourier transform ion-cyclotron resonance mass spectrometry (FT-ICR MS) is the only mass analyzer that can resolve the molecular complexity of natural organic matter at the level of elemental composition assignment. Here, we leverage the high dynamic range, resolving power, resistance to peak coalescence, and maximum ion number and ion trapping duration in a custom built, 21 tesla hybrid linear ion trap /FT-ICR mass spectrometer for a dissolved organic matter standard (Suwanne River Fulvic Acid). We compare the effect of peak-picking threshold (3σ, 4σ, 5σ, and 6σ) on number of elemental composition assignments, mass measurement accuracy, and dynamic range for a 6.3 s transient across the mass range of m/z 200−1200 that comprises the highest achieved resolving power broadband FT-ICR mass spectrum collected to date. More than 36 000 species are assigned with signal magnitude greater than 3σ at root-mean-square mass error of 36 ppb, the most species identified reported to date for dissolved organic matter. We identify ^{18}O and ^{17}O isotopologues and resolve isobaric overlaps on the order of a few electrons across a wide mass range (up to m/z 1000) leveraging mass resolving powers (3 000 000 at m/z 200) only achievable by 21 T FT-ICR MS and increased by ∼30% through absorption mode data processing. Elemental compositions unique to the 3σ span a wide compositional range of aromaticity not detected at higher peak-picking thresholds. Furthermore, we leverage the high dynamic range at 21 T FT-ICR MS to provide a molecular catalogue of a widely utilized reference standard (SRFA) to the analytical community collected on the highest performing mass analyzer for complex mixture analysis to date. This instrument is available free of charge to scientists worldwide.

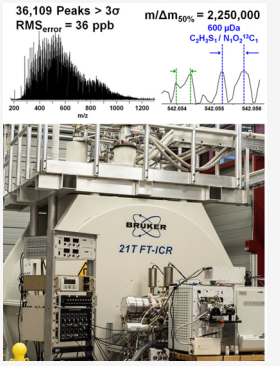

INTRODUCTION

Fourier transform ion-cyclotron resonance mass spectrometry (FT-ICR MS) is the only mass analyzer that can resolve the molecular complexity of natural organic matter at the level of elemental composition assignment, and has been applied to a wide range of natural systems (e.g., crude oil, petroleum, weathered oil, biofuels, permafrost, glacial thaw, emerging contaminants, food, and pyrogenic, dissolved, soil, and other natural organic matter).[1−8] However, experimental conditions including ionization source configuration, ion accumulation and transfer optics, detection cell geometry, excitation/detection parameters, and magnetic field strength present challenges for comparison of complex organic mixtures composition assignment between FT-ICR mass analyzers worldwide.

Recently, Hawkes et. al led an interlaboratory comparison of Suwanee River Fulvic Acid (SRFA),[9] a reference standard produced by the International Humic Substances Society (IHSS), a polydisperse, polyfunctional mixture of organic acids derived from allochthonous plant organic matter (i.e., a mixture of degraded tannins, lignins, carbohydrates, and lipids).[10−13] SRFA has been widely used as an analytical reference standard in the molecular characterization of dissolved organic matter (DOM) by negative-ion electrospray ionization due to its high acid content, and thus, it is one of the most widely used standards in analytical method development for complex organic mixture analysis. Most mass spectrometry studies on SRFA couple negative-ion electrospray ionization (ESI) to the mass analyzer, where ionization occurs through deprotonation reactions of highly abundant carboxylic acid moeities.[14] Across 10 commercial and custom-built FT-ICR mass analyzers cited, compositional differences (e.g., H/C and O/C ratios) derived from the number and type of assigned elemental compositions, ranged from ∼2000 peaks to ∼5000 peaks on instruments of varying magnetic field strength (7 to 15 T), that highlighted differences in all aspects of the mass analysis, (e.g., ion source configuration, ion accumulator/transfer hardware, ICR cell geometry, excitation/detection parameters, external/internal calibration equations, and data processing strategies and software). The resultant peak

Received: June 3, 2022
Accepted: July 25, 2022
Published: August 2, 2022

https://doi.org/10.1021/acs.analchem.2c02377
Anal. Chem. 2022, 94, 11382−11389

assignments varied in average oxidation state, saturation, and aromaticity by ∼15% for peaks common between the FT-ICR MS instruments, and even larger differences when considering peaks unique to each instrument, and demonstrates the impact of experimental parameters that impact ion detection for complex organic mixtures like DOM.

Many studies compare the molecular composition of DOM derived from negative-ion ESI FT-ICR MS across a range of marine,[15,16] terrestrial,[17,18] lacustrine,[19,20] and arctic field samples to the IHSS SRFA standard, which serves as a control for many biogeochemical applications.[21] Stenson et al. first characterized SRFA by negative-ESI FT-ICR MS at 9.4 T in 2003 and assigned ∼5000 elemental compositions.[14] Since 2003, numerous studies have characterized SRFA, including two interlaboratory comparisons to investigate the impact of various commercial and custom-built FT-ICR mass analyzers (Table S1).[9,22] Experimental conditions are critical to the mass spectral quality for complex organic mixture analysis at every stage of the FT-ICR MS experiment (e.g., ion source,[23] ion accumulator,[24] ion transfer optics and length,[24,25] rf transfer settings,[24] ICR cell geometry,[26,27] excitation waveform),[28] in addition to the magnetic field strength. Importantly, the method of FT-signal processing can significantly impact the mass spectral data quality, with absorption mode data resulting in ∼30% improvement in resolving power compared to magnitude mode.[29,30] Mass accuracy improves through application of an internal "walking" calibration and results in sub-ppm mass measurement error across thousands of elemental composition assignments.[31,32] All of the performance metrics of FT-ICR MS improve with higher magnetic field- mass resolving power and acquisition speed increase linearly, whereas mass accuracy, peak noncoalescence, and dynamic range increase quadratically with field strength.[33−35] In addition, the higher the magnetic field, the less susceptible an FT-ICR mass analyzer is to ion number-induced frequency shifts (space charge effects)[36] that can impact subsequent peak identification and calibration.[31,37,38]

Peak picking in mass spectrometry establishes the signal magnitude threshold for mass spectral peaks in a spectrum: peaks with signal magnitude above the threshold are considered for elemental composition assignment. Peak-picking at lower noise threshold results in higher peak counts but increases mass error due to peaks with lower S/N ratio, illustrating the trade-off between sensitivity and selectivity. Typical ranges for peak picking thresholds for FT-ICR MS analysis of complex organic mixtures range from three to six times the average baseline noise level (i.e., 3σ to 6σ).[9,14,39] The definition of limit of detection (LOD) has been defined by the following equation (IUPAC):[40]

$$x_{LOD} = x_{noise} + k\sigma_{noise}$$

Here, k is a numerical factor chosen for the desired confidence level. If we consider k = 3 (3σ), peaks above this threshold are identified at the 99.6% confidence interval provided the noise is normally distributed (Gaussian). Practically, this means that for peaks identified at this threshold, 997 instances of 1000 replicate measurements will be true analytes and not random noise fluctuation. Selecting k > 3 limits sensitivity while only enhancing selectivity marginally, as shown by the analysis herein. Previous studies report ∼2000 to 7500 elemental composition assignments at 3σ by 9.4 T FT-ICR MS in SRFA,[41,42] whereas comparison at 4σ identified ∼2000 to 5000 assignments from 10 FT-ICR mass analyzers (7 to 15 T).[9] At higher noise thresholds from 9.4 T data, ∼ 2500 assignments are reported at 5σ,[43,44] and ∼1500 to 9000 at 6σ.[45,46] To date, the highest number of peaks reported on SRFA results from 6σ peak picking and yields ∼13 000 elemental composition assignments at ∼60 ppb RMS mass error with 21 T FT-ICR MS.[46]

Once resolved and peak-picked, the tens of thousands of mass spectral peaks in a single DOM sample must be internally calibrated to result in sub-ppm mass error for accurate elemental composition assignment. Internal calibration on highly abundant homologous series within the sample itself result in the lowest mass error across a wide molecular weight range.[14,47] Internal calibration is based on the quadratic Ledford equation,[36] though other equations (e.g., linear, polynomial) and the "walking" calibration[31] have also been widely used. Current reports for mass measurement error range from ∼25−50 ppb to 2−5 ppm for DOM species by FT-ICR MS.[3,9,18,22,42,46]

Elemental composition assignment software for complex organic mixture FT-ICR MS include open-source software (e.g., UltraMassExplorer,[48] Formularity[49]), open-source R, Python, C++, or MATLAB molecular formula assignment tools (e.g., CoreMS,[50] CIA,[51] MFAssignR,[52] TRFu,[53] ICBM-OCEAN[54]), and molecular formula assignment software (e.g., PetroOrg/EnviroOrg,[55] Composer[56]). Each method involves the differentiation of elemental composition assignments based on Kendrick mass defect analysis,[57] elemental constraints, mass error, and isotope confirmation to increase reliability.

The custom-built, 21 T FT-ICR mass spectrometer at the NHMFL leads the world in complex mixture analysis, and routinely achieves resolving power in excess of 1 500 000 (at m/z 400), the lowest mass measurement error (10−50 ppb RMS error), and highest dynamic range of any mass analyzer,[46,58,59] and is fitted with automatic gain control (AGC) to minimize scan to scan variations in ion number,[60,61] which enables identification of species that differ in mass by roughly the mass of an electron.[46,59] The increased dynamic range (ratio of highest to lowest peak) enables simultaneous detection of low and high abundant species without distorting relative ion abundances.[33]

Here, we leverage the high dynamic range, mass resolving power, resistance to peak coalescence, maximum ion number, and trapping duration in a 21 T FT-ICR MS instrument for complex organic mixture analysis.[34] We compare the impact of peak picking threshold (3σ, 4σ, 5σ, and 6σ) on number of elemental composition assignments, mass measurement accuracy, mass resolving power, and dynamic range for the highest resolving power broadband FT-ICR mass spectrum collected to date on dissolved organic matter ($\Delta m/m_{50\%}$ = 3 000 000 at m/z 200 (6.3 s transient from m/z 200−1200). We identify ^{18}O and ^{17}O isotopologues for oxygenated species in a broadband mass spectrum for first time, and identify new isobaric overlaps in DOM on the order of a few electron mass differences, only possible due to mass resolving power achieved by 21 T FT-ICR MS. Furthermore, mass resolving power is increased by ∼30% through absorption mode data processing, and increased dynamic range provides a molecular catalogue for a standard reference material widely used in environmental applications to the analytical community. The 21 T FT-ICR instrument is available free of charge to scientists worldwide.

https://doi.org/10.1021/acs.analchem.2c02377
Anal. Chem. 2022, 94, 11382−11389

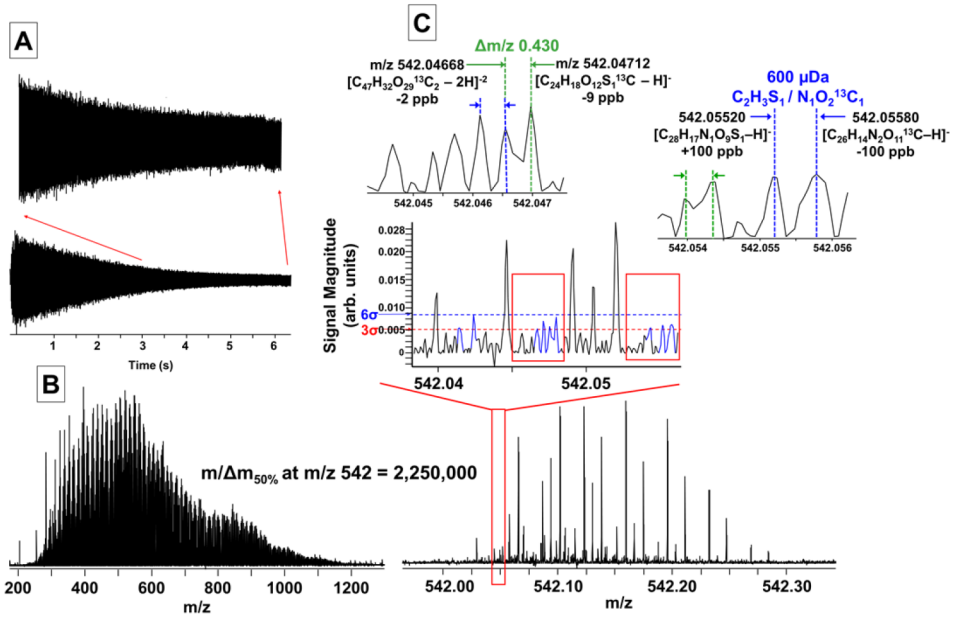

Figure 1. Negative-ion ESI 21 T FT-ICR mass spectrum of the Suwannee River Fulvic Acid (SRFA) standard with insets depicting mass spectral complexity, resolving power, and dynamic range. (A) Transient signal averaged over 560 scans and a 6.3s acquisition window with a zoomed inset. (B) broadband FT-ICR mass spectrum between m/z 200−1200, centered at m/z 542. (C) 300 mDa mass scale-expanded segment from m/z 542.0−542.3, with achieved resolving power, $m/\Delta m_{50\%}$ ($\Delta m_{50\%}$ = the full mass spectral peak width at half-maximum peak height) of 2 250 000 at m/z 542.[34] A mass scale-expanded zoom with thresholds designated between 3σ (red) and 6σ (blue) is demonstrated within this segment for peaks considered as mass spectral peaks (as opposed to noise). Portions of the spectrum are expanded further in insets for peaks identified in the 3σ between m/z 542.046−542.048 and 542.054−542.056 that illustrate the resolution of species that differ in mass by roughly the mass of an electron (548 μDa).

Table 1. Resolving Power, Dynamic Range, and Number of Elemental Compositions Assigned by Heteroatom Class as a Function of Peak-Picking Threshold for Suwannee River Fulvic Acid (SRFA)

	resolving power ($m/\Delta m_{50\%}$) at m/z 400	dynamic range	total	CHO (w/isotopes and Na adducts)	CHNO (w/isotopes)	CHOS (w/isotopes)	CHNOS
SRFA 3σ	2960218	374.2	36109	23097	8776	3840	396
SRFA 4σ	2973674	275.6	32855	22736	7425	2541	153
SRFA 5σ	2993832	238.0	29816	21286	6227	2244	59
SRFA 6σ	3019947	191.7	23641	17353	4850	1434	4

EXPERIMENTAL METHODS

Suwannee River Fulvic Acid (SRFA) standard obtained from the IHSS (https://humic-substances.org/the-third-batch-of-suwannee-river-humic-and-fulvic-acids/) was diluted in HPLC grade methanol (JT. Baker Scientific, San Jose, California) without further modification prior to negative-ion ESI 21 T FT-ICR MS analysis.[10−13] Peaks with signal magnitude greater than 3, 4, 5, and 6 times the baseline root-mean-square (rms) noise at m/z 500 were exported to peak lists, phase-corrected,[62] and internally calibrated based on the "walking" calibration method.[31] Mass spectral peaks were assigned elemental compositions that contain carbon (C), hydrogen (H), oxygen (O), nitrogen (N), and sulfur (S) and visualized with PetroOrg software.[55] Molecular formula assignments with an error >0.4 parts-per-million were discarded, and only heteroatom classes with a combined relative abundance of ≥0.15% of the total were considered. Complete experimental details and data processing methodology can be found in the Supporting Information. Absorption-mode 21 T FT-ICR mass spectra files and assigned elemental compositions are publicly available via the Open Science Framework at https://osf.io/zgx3y/ (DOI: 10.17605/OSF.IO/ZGX3Y).

RESULTS AND DISCUSSION

Resolving Power >2 000 000 and High Dynamic Range at 21 T Identifies New Isobaric Species. Figure 1 shows a broadband negative-ion electrospray ionization of SRFA collected on a custom-built 21T FT-ICR mass spectrometer that spans from 200 < m/z < 1200, centered at m/z 540.[39,46,58] More than 560 scans were signal averaged over a 6.3 s acquisition period with signal lasting the entire detection period, and achieved resolving power of $m/\Delta m_{50\%}$ (in which $\Delta m_{50\%}$ = mass spectral peak width at half-maximum peak height) of 2 250 000 at m/z 542. The mass spectral complexity is highlighted in the mass-scale expanded zoom inset of 0.3 Da (542.0 < m/z < 542.3).

Figure 1 further illustrates the improved dynamic range of the 21 T, demonstrated with a mass-scale zoom inset at m/z 542 (top right) with peak-picking thresholds annotated at 3σ (red) and 6σ (blue). Peak-picking at three times the baseline noise level (3σ) exports lower abundance peaks to a peak list where isobaric species differ in mass by $\Delta m/z$ 0.000430 ($[C_{47}H_{32}O_{29}{}^{13}C_2{-}H]^{2-}$ and $[C_{24}H_{18}O_{12}S_1{}^{13}C{-}H]^{-}$) (top, green arrows)[46] at sub 10 ppb mass error. Furthermore, isobaric species with the same nominal mass (59 Da) that differ in exact mass by 600 μDa (roughly the mass of an

https://doi.org/10.1021/acs.analchem.2c02377
Anal. Chem. 2022, 94, 11382−11389

electron, 548 μDa) and differ in elemental composition by $C_2H_3S_1$ and $N_1O_2{}^{13}C$ are baseline resolved with a mass error of ±100 ppb. A shift in experimental mass difference is likely caused by an unresolved peak or shoulder at high frequency on m/z 542.05580.

Table 1 shows resolving power (i.e., $m/m_{50\%}$ averaged from peaks between m/z 395−405), dynamic range (i.e., the maximum peak height divided by the minimum peak height of the most and least abundant assigned peaks, respectively), and number of peaks assigned elemental compositions in total and by heteroatom class from the SRFA spectrum at each peak-picking threshold. This mass spectrum results in the highest achieved resolving power for direct infusion mass spectrometry of dissolved organic matter to date, with achieved resolving power of ∼3 000 000 at m/z 400 at each peak-picking threshold. The dynamic range decreases by nearly a factor of 2 between the 3σ and 6σ thresholds (374.2 to 191.7, respectively) and impacts the number of assignments, from 36 109 (3σ) to 23 641 (6σ). The CHNO assignments decreased by ∼45% from the 3σ to the 6σ (from 8776 to 4850), and CHOS assignments decreased by ∼63% (from 3840 to 1434). In comparison, the CHO assignments decreased only ∼25% at 6σ (from 23097 to 17353). Nitrogen and sulfur heteroatom classes (i.e., CHNOS) further decreased at 6σ, with CHNOS assignments decreased by ∼99% (396 to 4). This decrease is also apparent in assignments containing multiple nitrogen, seen in Figure S1.

Resolution and Identification of ^{18}O and ^{17}O Isotopologues in Broadband SRFA 21 T FT-ICR MS. The high dynamic range, sub-ppm mass error, and >2 000 000 resolving power of the 21 T enable the first resolution, identification, and isotopic confirmation of oxygen isotopologues in dissolved organic matter. Figure 2 shows a zoom inset at m/z 505.09878 that corresponds to the monoisotopic oxygen species $[C_{23}H_{22}O_{13}-H]^-$. The theoretical mass difference between ^{16}O (natural abundance 99.75%) and ^{17}O (0.038%) is +1.00421 Da and ^{16}O and ^{18}O (0.2%) is +2.00424 Da, and both ^{18}O and ^{17}O isotopologues are detected and assigned. Careful examination of the ^{17}O isotopologues reveals a 0.87 mDa mass difference sufficiently resolved ($m/\Delta m_{50\%}$ = 2 600 000−2 800 000) between the ^{13}C isotopologue $[C_{22}H_{22}O_{13}{}^{13}C-H]^-$ (S/N 172, 40 ppb) and ^{17}O $[C_{23}H_{22}O_{12}{}^{17}O-H]^-$ (S/N 3, 60 ppb).

Peak-Picking Influences Isobaric Species Identification. Figure 3 shows the number of isobaric overlaps detected from elemental compositions assigned at 3σ, 4σ, 5σ, and 6σ from SRFA. Three overlaps are highlighted: $NO_2{}^{13}C/C_2H_3S$ (59 Da nominal mass and differing in theoretical exact mass by 0.71 mDa), $H_2O_3{}^{13}C_2/C_4N_2$ (76 Da nominal mass and differing in theoretical exact mass by 0.96 mDa), and $C_2N_2/H_2O_2{}^{18}O$ (52 Da nominal mass and differing in theoretical exact mass by 1.51 mDa). Each image plots the number of overlaps in assigned peaks versus the experimental observed mass difference between m/z for isobaric species. The dashed line shows the theoretical mass difference, calculated from atomic weight. A complete list of all identified isobaric overlaps below $\Delta m/z$ 0.03638 can be found in Table S2. The newly identified isobaric overlaps include thousands of species that differ in mass by 1−2 electrons (M_{e-} = 548 μDa),[63] resolved for the first time in SRFA. For instance, the $NO_2{}^{13}C/C_2H_3S$ overlap was the most identified mass split above 3σ (1076 counts), followed by 4σ (882 counts), 5σ (704 counts), and 6σ (506 counts). As expected newly identified isobaric overlaps

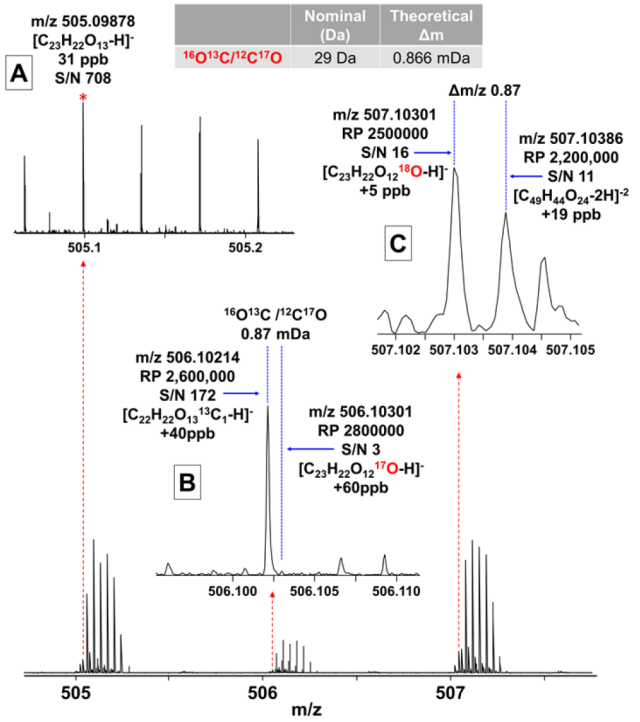

Figure 2. Mass-scale expanded inset (bottom) for 505 < m/z < 507 derived from broadband 21 T negative-ion ESI FT-ICR mass spectrum of Suwannee River Fulvic Acid to illustrate mass resolution that enables identification of oxygen isotopes confirmed by resolution and detection of isotopic fine structure (^{13}C, ^{17}O, and ^{18}O isotopologues) with sub-ppb mass error. (A) The assignment of the monoisotopic species $[C_{23}H_{22}O_{13}-H]^-$ at m/z 505.09878 and signal-to-noise ratio (S/N) of 708. (B) Assignment of $[C_{22}H_{22}O_{13}{}^{13}C_1-H]^-$ and $[C_{23}H_{22}O_{12}{}^{17}O-H]^-$ isotopologues, at S/N values of 172 and 3. Identification of ^{17}O species for the first time occurs due to achieved resolving power >2 600 000 that enables resolution of isobaric species that differ in elemental composition by $^{12}C^{17}O$ versus $^{16}O^{13}C$, with an experimental mass difference of 0.87 mDa. The theoretical mass difference between $^{12}C^{17}O$ and $^{16}O^{13}C$ is 0.866 mDa. (C) Assignment of the $[C_{23}H_{22}O_{12}{}^{18}O-H]^-$ isotopologue (S/N = 16) resolved from $[C_{49}H_{44}O_{24}-2H]^{2-}$ (S/N = 11).

that include nonoxygen heteroatoms and ^{13}C or ^{18}O isotopes were the most influenced by the peak-picking threshold. This can also be seen in Figure S2, where the highest number of nitrogen- and sulfur-containing overlaps were identified at 3σ, and lowest at 6σ. In comparison, the CHO-containing overlaps increases at 3σ with a maximum at 4σ, and then reached a minimum at 6σ. This is due to the inclusion or exclusion of low abundance heteroatom or isotope-containing assignments that plot between CHO-containing overlaps.

Resolving Power >2 000 000 Resolves Isobaric Overlaps. Figure 4 displays the counts of each isobaric overlap at 3σ from Figure 3, separated by m/z bins every m/z 100 (e.g., m/z 300−400, m/z 400−500). Plots of the isobaric overlaps binned by m/z at 4σ, 5σ, and 6σ can be seen in Figure S3 and follow a similar distribution. For instance, with the 0.71 mDa isobaric overlap, the minimum counts were on the low (300 < m/z < 400) and high (900 < m/z < 1000) molecular weight range with 31 (low) and 32 (high) counts. The maximum count occurred in the center of the molecular weight distribution (500 < m/z < 600) with 328 counts. This highlights the achieved resolving power at higher m/z that can resolve and identify species that differ in mass on the order of

https://doi.org/10.1021/acs.analchem.2c02377
Anal. Chem. 2022, 94, 11382−11389

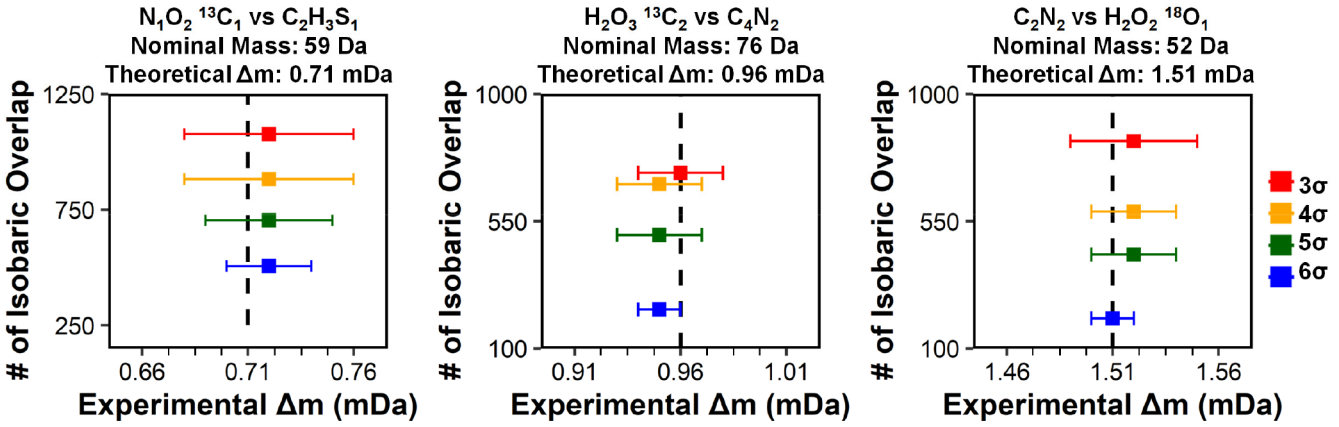

Figure 3. Selected isobaric overlaps identified and counted in each sample, with each point colored by peak-picking threshold. Points correspond to the average mass difference, with lines denoting standard deviation for counted experimental overlaps. The theoretical mass difference is indicated by the dotted center line in each plot. Each *x*-axis spans ±0.0001 Da. For a complete list of isobaric overlaps below a mass difference of *m/z* 0.03638, see Table S2.

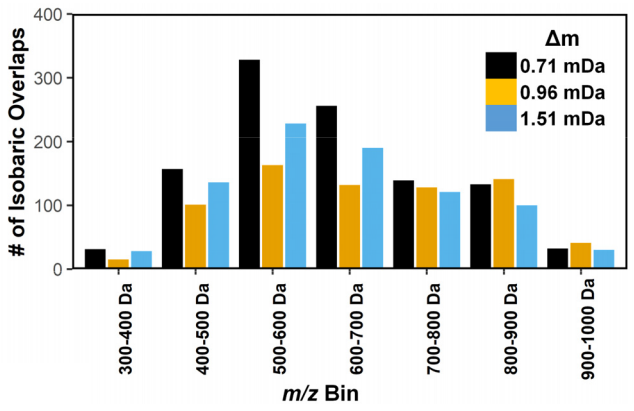

Figure 4. Number of isobaric overlaps in SRFA peak-picked at 3σ identified in Figure 3 and binned by every *m/z* 100, up to *m/z* 1000. Bars are colored by theoretical isobaric overlap that each count was associated with. For the 4σ, 5σ, and 6σ bar plots of the selected isobaric overlaps, see Figure S3.

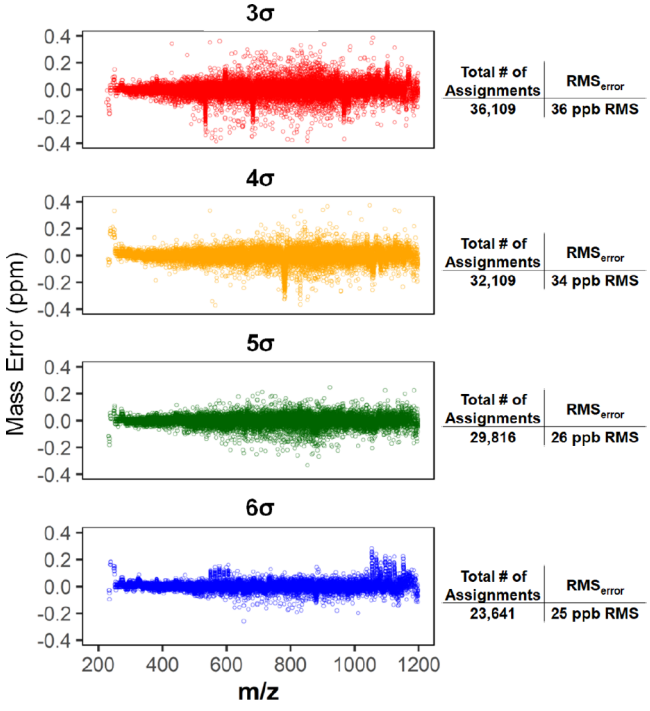

Figure 5. Elemental compositions assigned in each of the SRFA samples plotted by mass error versus *m/z*. RMS$_{error}$ and total number of assignments derived from 3σ, 4σ, 5σ, and 6σ data sets are also tabulated. For assigned peaks by quartile, see Table S3.

an electron up to ∼900−1000 Da. The identification of these species also occurred at high *m/z* at 5σ and 6σ, but at lower counts. This has been directly compared recently with the *m/z* 0.000430 mass difference visualized in Figure 1, which could not be resolved at *m/z* ∼ 600 in SRFA on a 9.4 T FT-ICR MS.[46] Isobaric overlaps were identified throughout this study and are resolved up to *m/z* 1000.

Elemental Composition Assignments and RMS Mass Error. The mass measurement error as a function of molecular weight for assignments derived from 3σ, 4σ, 5σ, and 6σ is shown in Figure 5. At 6σ, more than 23 000 species are assigned with 25 ppb RMS error, whereas 3σ results in a 52% increase in the number of assignments (36 000) with 36 ppb RMS error. This slight increase of 11 ppb in RMS error can be accounted for in the assignment of more species with lower *S/N* in 3σ. Table S3 compiles the number of assignments at each % relative abundance and RMS error for all four data sets. Specifically, ∼10 000 more assignments with signal magnitude lower than 25% total relative abundance at 3σ are assigned that have lower *S/N* and higher mass error (31 ppb) compared to 6σ. Therefore, changes to RMS$_{error}$ can be attributed primarily to the bottom 25% abundance quartile, which includes nitrogen and sulfur species (Table 1). Importantly, with 21 T FT-ICR MS, lower abundant species at 3σ are assigned elemental compositions at ∼20−40 ppb RMS error and expand the compositional window for identified species by ∼50%.

Detection at 3σ Extends Compositional Coverage. The increase in detected species impacts the number and compositional range for assigned species based on stoichiometry. Visualization of DOM compositional range often includes van Krevelen diagrams that plot atomic H/C versus O/C ratio to approximate oxidation state, compositional information to biomolecular precursors,[45,64] and calculate hydrogen deficiency (e.g., DBE, double bond equivalents, the number of rings plus double bonds to carbon, DBE = $C - h/2 + n/2 + 1$,[65] or aromaticity index, AI) to approximate biolability.[66]

https://doi.org/10.1021/acs.analchem.2c02377
Anal. Chem. 2022, 94, 11382−11389

Figure 6A shows H/C versus O/C for neutral species unique to the 3σ when compared to the 6σ. Points are colored by AI:

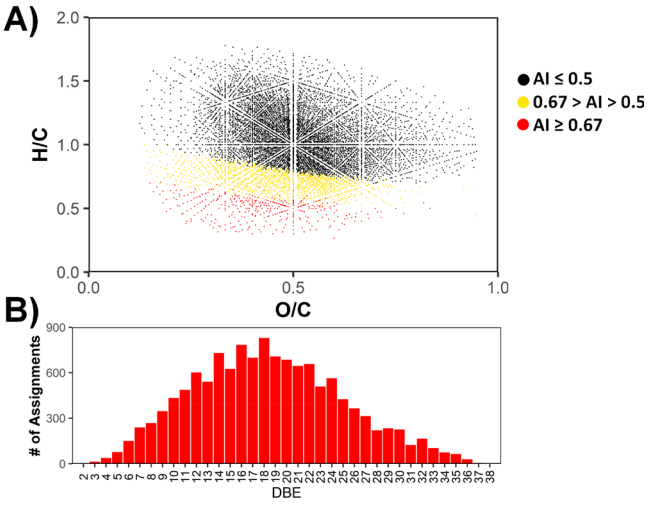

Figure 6. Assignments unique to the 3σ plotted by atomic ratios in a van Krevelen diagram and by DBE. (A) H/C versus O/C ratios of the assigned molecular formulas in a van Krevelen diagram, where assignments are colored by the aromaticity index: nonaromatic (black, AI ≤ 0.5), aromatic (gold, 0.67 > AI > 0.5), and condensed aromatic (red, AI ≥ 0.67). (B) Number of unique assignments to the 3σ binned by rings-plus-double-bond-equivalents (DBE).

nonaromatic (black, AI ≤ 0.5), aromatic (gold, 0.67 > AI > 0.5), and condensed aromatic (red, AI ≥ 0.67). A total of 12 937 assignments were unique to the 3σ data set, with 12 933 (99.9%) peaks belonging to the <25% relative abundance quartile. Species assigned only at 3σ encompass a large compositional space from H/C ∼ 0.4−1.5 and O/C ∼ 0.2−0.8. Figure 6B shows the number of unique assignments in the 3σ as a function of DBE. Assignments unique to the 3σ range from 3 to 36 DBE, which highlights the large range of aromaticity only available at 3σ.

CONCLUSIONS

The SRFA spectrum highlighted here represents a unique experiment in which the highest resolving power, mass measurement accuracy, and dynamic range to date is reported for a widely utilized reference material. Assignment of ^{18}O and ^{17}O isotopologues was enabled by lowering the peak-picking threshold and identified thousands of isobaric overlaps that differ in mass by 1−2 electrons. Enhanced sensitivity with respect to peak detection and subsequent elemental composition assignment is achieved at peak detection threshold of 3σ. Lowering the peak detection threshold to 3σ does not appreciably affect selectivity of the measurement in terms of accumulation of false assignments or unidentified peaks ("no-hits"). In fact, setting a more stringent peak picking threshold (>3σ) arbitrarily limits the depth of compositional assignment, effectively leaving high confidence peaks out of the assignment process. Therefore, we report a 3σ peak picking threshold that identifies a wider range of species that impact calculations based on elemental compositions (e.g., oxidation state, DBE, AI). will more accurately represent the bulk NOM with inclusion of lower abundance species not detected by other mass analyzers and provide a more comprehensive representation of natural organic matter by FT-ICR MS. These data are provided via the Open Science Framework as reference data set for the scientific community.

ASSOCIATED CONTENT

Supporting Information

The Supporting Information is available free of charge at https://pubs.acs.org/doi/10.1021/acs.analchem.2c02377.

Supplementary tables and figures describing previous literature, isobaric overlaps, peak assignments, and a description of the FT-ICR MS methodology (PDF)

AUTHOR INFORMATION

Corresponding Authors

Amy M. McKenna − *National High Magnetic Field Laboratory, Ion Cyclotron Resonance Facility, Florida State University, Tallahassee, Florida 32310-4005, United States; Department of Soil and Crop Sciences, Colorado State University, Fort Collins, Colorado 80523-1170, United States;* orcid.org/0000-0001-7213-521X; Phone: +1 850 644 4809; Email: mckenna@magnet.fsu.edu

Thomas Borch − *Department of Chemistry, Colorado State University, Fort Collins, Colorado 80523, United States; Department of Soil and Crop Sciences, Colorado State University, Fort Collins, Colorado 80523-1170, United States*; Phone: +1 970 491 6235; Email: Thomas.Borch@ColoState.EDU

Authors

William Bahureksa − *Department of Chemistry, Colorado State University, Fort Collins, Colorado 80523, United States;* orcid.org/0000-0003-3056-3595

Robert B. Young − *Chemical Analysis & Instrumentation Laboratory, New Mexico State University, Las Cruces, New Mexico 88003, United States;* orcid.org/0000-0001-7485-0604

Chad. R. Weisbrod − *National High Magnetic Field Laboratory, Ion Cyclotron Resonance Facility, Florida State University, Tallahassee, Florida 32310-4005, United States;* orcid.org/0000-0001-5324-4525

Greg T. Blakney − *National High Magnetic Field Laboratory, Ion Cyclotron Resonance Facility, Florida State University, Tallahassee, Florida 32310-4005, United States;* orcid.org/0000-0002-4205-9866

Complete contact information is available at: https://pubs.acs.org/10.1021/acs.analchem.2c02377

Author Contributions

The manuscript was written through contributions of all authors. All authors have given approval to the final version of the manuscript.

Notes

The authors declare no competing financial interest.

ACKNOWLEDGMENTS

The authors thank Christopher L. Hendrickson, Daniel MacIntosh, and John P. Quinn for helpful discussions and design and maintenance of the 21 T instrument. The ICR User Facility at the National High Magnetic Field Laboratory is and open-access user facility supported by the National Science Foundation Division of Chemistry and Division of Materials Research through Grant DMR-1644779, and the State of Florida. The authors also acknowledge support to Thomas

Borch by the National Science Foundation (2114868) and the USDA National Institute of Food Agriculture through AFRI Grant No. 2021-67019-34608 and Grant No. 2021-67019-33726.

REFERENCES

(1) Liberatore, H. K.; Westerman, D. C.; Allen, J. M.; Plewa, M. J.; Wagner, E. D.; McKenna, A. M.; Weisbrod, C. R.; McCord, J. P.; Liberatore, R. J.; Burnett, D. B.; et al. *Environ. Sci. Technol.* **2020**, *54* (15), 9374−9386.
(2) McKenna, A. M.; Donald, L. J.; Fitzsimmons, J. E.; Juyal, P.; Spicer, V.; Standing, K. G.; Marshall, A. G.; Rodgers, R. P. *Energy Fuels* **2013**, *27* (3), 1246−1256.
(3) Wagner, S.; Riedel, T.; Niggemann, J.; Vähätalo, A. V.; Dittmar, T.; Jaffé, R. *Environ. Sci. Technol.* **2015**, *49* (23), 13798−13806.
(4) Bahureksa, W.; Tfaily, M. M.; Boiteau, R. M.; Young, R. B.; Logan, M. N.; McKenna, A. M.; Borch, T. *Environ. Sci. Technol.* **2021**, *55* (14), 9637−9656.
(5) Young, R. B.; Pica, N. E.; Sharifan, H.; Chen, H.; Roth, H. K.; Blakney, G. T.; Borch, T.; Higgins, C. P.; Kornuc, J. J.; McKenna, A. M.; et al. *Environ. Sci. Technol.* **2022**, *56* (4), 2455−2465.
(6) Patzner, M. S.; Logan, M.; McKenna, A. M.; Young, R. B.; Zhou, Z.; Joss, H.; Mueller, C. W.; Hoeschen, C.; Scholten, T.; Straub, D.; et al. *Commun. Earth Environ.* **2022**, *3* (1), 1−14.
(7) Bahureksa, W.; Young, R. B.; McKenna, A. M.; Chen, H.; Thorn, K. A.; Rosario-Ortiz, F. L.; Borch, T. *Environ. Sci. Technol.* **2022**, *56*, 4597.
(8) Hemmler, D.; Roullier-Gall, C.; Marshall, J. W.; Rychlik, M.; Taylor, A. J.; Schmitt-Kopplin, P. *Sci. Rep.* **2018**, *8* (1), 1−10.
(9) Hawkes, J. A.; D'Andrilli, J.; Agar, J. N.; Barrow, M. P.; Berg, S. M.; Catalán, N.; Chen, H.; Chu, R. K.; Cole, R. B.; Dittmar, T.; et al. *Limnol. Oceanogr. Methods* **2020**, *18* (6), 235−258.
(10) Leenheer, J. A.; Brown, G. K.; Maccarthy, P.; Cabaniss, S. E. *Environ. Sci. Technol.* **1998**, *32* (16), 2410−2416.
(11) Olk, D. C.; Bloom, P. R.; Perdue, E. M.; McKnight, D. M.; Chen, Y.; Farenhorst, A.; Senesi, N.; Chin, Y.-P.; Schmitt-Kopplin, P.; Hertkorn, N.; et al. *J. Environ. Qual.* **2019**, *48* (2), 217−232.
(12) Aiken, G. R. Isolation and Concentration Techniques for Aquatic Humic Substances. In *Humic substances in soil, sediment and water: geochemistry and isolation*; Aiken, G. R., McKnight, D. M., Wershaw, R. L., Maccarthy, P., Eds.; Wiley-Interscience: New York, 1985.
(13) International Humic Substances Society. Isolation of IHSS Samples. https://humic-substances.org/isolation-of-ihss-samples/ (accessed Jun 6, 2021).
(14) Stenson, A. C.; Marshall, A. G.; Cooper, W. T. *Anal. Chem.* **2003**, *75* (6), 1275−1284.
(15) Kellerman, A. M.; Guillemette, F.; Podgorski, D. C.; Aiken, G. R.; Butler, K. D.; Spencer, R. G. M. *Environ. Sci. Technol.* **2018**, *52* (5), 2538−2548.
(16) Reemtsma, T.; These, A.; Linscheid, M.; Leenheer, J.; Spitzy, A. *Environ. Sci. Technol.* **2008**, *42* (5), 1430−1437.
(17) Kurek, M. R.; Poulin, B. A.; Mckenna, A. M.; Spencer, R. G. M. *Environ. Sci. Technol.* **2020**, *54* (24), 16249−16259.
(18) Koch, B. P.; Witt, M.; Engbrodt, R.; Dittmar, T.; Kattner, G. *Geochim. Cosmochim. Acta* **2005**, *69* (13), 3299−3308.
(19) Brezonik, P. L.; Bloom, P. R.; Sleighter, R. L.; Cory, R. M.; Khwaja, A. R.; Hatcher, P. G. *J. Environ. Chem. Eng.* **2015**, *3* (4), 2982−2990.
(20) Kellerman, A. M.; Kothawala, D. N.; Dittmar, T.; Tranvik, L. J. *Nat. Geosci.* **2015**, *8* (6), 454−457.
(21) Wagner, S.; Dittmar, T.; Jaffé, R. *Org. Geochem.* **2015**, *79*, 21−30.
(22) Zherebker, A.; Kim, S.; Schmitt-Kopplin, P.; Spencer, R. G. M.; Lechtenfeld, O.; Podgorski, D. C.; Hertkorn, N.; Harir, M.; Nurfajin, N.; Koch, B.; et al. *Pure Appl. Chem.* **2020**, *92* (9), 1447−1467.
(23) Chen, Y.; Leach, F. E.; Kaiser, N. K.; Dang, X.; Ibrahim, Y. M.; Norheim, R. V.; Anderson, G. A.; Smith, R. D.; Marshall, A. G. *J. Mass Spectrom.* **2015**, *50* (1), 280−284.
(24) Kaiser, N. K.; Savory, J. J.; Hendrickson, C. L. *J. Am. Soc. Mass Spectrom.* **2014**, *25* (6), 943−949.
(25) Wilcox, B. E.; Hendrickson, C. L.; Marshall, A. G. *J. Am. Soc. Mass Spectrom.* **2002**, *13* (11), 1304−1312.
(26) Boldin, I. A.; Nikolaev, E. N. *Rapid Commun. Mass Spectrom.* **2011**, *25* (1), 122−126.
(27) Chen, T.; Beu, S. C.; Kaiser, N. K.; Hendrickson, C. L. *Rev. Sci. Instrum.* **2014**, *85* (6), 066107.
(28) Kaiser, N. K.; McKenna, A. M.; Savory, J. J.; Hendrickson, C. L.; Marshall, A. G. *Anal. Chem.* **2013**, *85* (1), 265−272.
(29) Kilgour, D. P. A.; Wills, R.; Qi, Y.; O'Connor, P. B. *Anal. Chem.* **2013**, *85* (8), 3903−3911.
(30) Beu, S. C.; Blakney, G. T.; Quinn, J. P.; Hendrickson, C. L.; Marshall, A. G. *Anal. Chem.* **2004**, *76* (19), 5756−5761.
(31) Savory, J. J.; Kaiser, N. K.; McKenna, A. M.; Xian, F.; Blakney, G. T.; Rodgers, R. P.; Hendrickson, C. L.; Marshall, A. G. *Anal. Chem.* **2011**, *83* (5), 1732−1736.
(32) Wong, R. L.; Amster, I. J. *J. Am. Soc. Mass Spectrom.* **2006**, *17* (12), 1681−1691.
(33) Bowman, A. P.; Blakney, G. T.; Hendrickson, C. L.; Ellis, S. R.; Heeren, R. M. A.; Smith, D. F. *Anal. Chem.* **2020**, *92* (4), 3133−3142.
(34) Marshall, A. G.; Hendrickson, C. L.; Jackson, G. S. *Mass Spectrom. Rev.* **1998**, *17*, 1−35.
(35) Marshall, A. G.; Guan, S.; Eyler, J. R. *Rapid Commun. Mass Spectrom.* **1996**, *10* (14), 1814−1818.
(36) Ledford, E. B.; Rempel, D. L.; Gross, M. L. *Anal. Chem.* **1984**, *56* (14), 2744−2748.
(37) Xiang, X.; Grosshans, P. B.; Marshall, A. G. *Int. J. Mass Spectrom. Ion Process.* **1993**, *125* (1), 33−43.
(38) Wong, R. L.; Amster, I. J. *Int. J. Mass Spectrom.* **2007**, *265* (2−3), 99−105.
(39) Shaw, J. B.; Lin, T. Y.; Leach, F. E.; Tolmachev, A. V.; Tolić, N.; Robinson, E. W.; Koppenaal, D. W.; Paša-Tolić, L. *J. Am. Soc. Mass Spectrom.* **2016**, *27* (12), 1929−1936.
(40) IUPAC. *Compendium of Chemical Terminology (the "Gold Book")*, 2nd ed.; McNaught, A. D., Wilkinson, A., Eds.; Blackwell Scientific Publications: Oxford, U.K., 1997; DOI: 10.1351/goldbook.
(41) Koch, B. P.; Dittmar, T.; Witt, M.; Kattner, G. *Anal. Chem.* **2007**, *79* (4), 1758−1763.
(42) Hertkorn, N.; Frommberger, M.; Witt, M.; Koch, B. P.; Schmitt-Kopplin, P.; Perdue, E. M. *Anal. Chem.* **2008**, *80* (23), 8908−8919.
(43) Kido Soule, M. C.; Longnecker, K.; Giovannoni, S. J.; Kujawinski, E. B. *Org. Geochem.* **2010**, *41* (8), 725−733.
(44) Minor, E. C.; Steinbring, C. J.; Longnecker, K.; Kujawinski, E. B. *Org. Geochem.* **2012**, *43*, 1−11.
(45) D'Andrilli, J.; Foreman, C. M.; Marshall, A. G.; McKnight, D. M. *Org. Geochem.* **2013**, *65*, 19−28.
(46) Smith, D. F.; Podgorski, D. C.; Rodgers, R. P.; Blakney, G. T.; Hendrickson, C. L. *Anal. Chem.* **2018**, *90* (3), 2041−2047.
(47) Hughey, C. A.; Hendrickson, C. L.; Rodgers, R. P.; Marshall, A. G.; Qian, K. *Anal. Chem.* **2001**, *73* (19), 4676−4681.
(48) Leefmann, T.; Frickenhaus, S.; Koch, B. P. *Rapid Commun. Mass Spectrom.* **2019**, *33* (2), 193−202.
(49) Tolić, N. T.; Liu, Y.; Liyu, A.; Shen, Y.; Tfaily, M. M.; Kujawinski, E. B.; Longnecker, K.; Kuo, L.-J. J.; Robinson, E. W.; et al. *Anal. Chem.* **2017**, *89* (23), 12659−12665.
(50) Corilo, Y. E.; Kew, W. R.; McCue, L. A. *EMSL-Computing/CoreMS: CoreMS 1.0.0* **2021**, DOI: 10.5281/ZENODO.4641553.
(51) Kujawinski, E. B.; Behn, M. D. *Anal. Chem.* **2006**, *78* (13), 4363−4373.
(52) Schum, S. K.; Brown, L. E.; Mazzoleni, L. R. *Environ. Res.* **2020**, *191*, 110114.
(53) Fu, Q.-L. L.; Fujii, M.; Riedel, T. *Anal. Chim. Acta* **2020**, *1125*, 247−257.

(54) Merder, J.; Freund, J. A.; Feudel, U.; Hansen, C. T.; Hawkes, J. A.; Jacob, B.; Klaproth, K.; Niggemann, J.; Noriega-Ortega, B. E.; Osterholz, H.; et al. *Anal. Chem.* **2020**, *92* (10), 6832−6838.
(55) Corilo, Y. E. *PetroOrg Software, Florida State University*: Omics LLC: Tallahassee, Fl, 2014.
(56) Stranz, D. *Composer64*, v1. 5.0; Sierra Anal. Inc.: 2015.
(57) Fouquet, T.; Sato, H. *Anal. Chem.* **2017**, *89* (5), 2682−2686.
(58) Hendrickson, C. L.; Quinn, J. P.; Kaiser, N. K.; Smith, D. F.; Blakney, G. T.; Chen, T.; Marshall, A. G.; Weisbrod, C. R.; Beu, S. C. *J. Am. Soc. Mass Spectrom.* **2015**, *26* (9), 1626−1632.
(59) Roth, H. K.; Borch, T.; Young, R. B.; Bahureksa, W.; Blakney, G. T.; Nelson, A. R.; Wilkins, M. J.; McKenna, A. M. *Anal. Chem.* **2022**, *94* (6), 2973−2980.
(60) Page, J. S.; Bogdanov, B.; Vilkov, A. N.; Prior, D. C.; Buschbach, M. A.; Tang, K.; Smith, R. D. *J. Am. Soc. Mass Spectrom.* **2005**, *16* (2), 244−253.
(61) Williams, D. K.; Muddiman, D. C. *Anal. Chem.* **2007**, *79* (13), 5058−5063.
(62) Xian, F.; Hendrickson, C. L.; Blakney, G. T.; Beu, S. C.; Marshall, A. G. *Anal. Chem.* **2010**, *82* (21), 8807−8812.
(63) Audi, G.; Bersillon, O.; Blachot, J.; Wapstra, A. H. *Nucl. Phys. A* **2003**, *729* (1), 3−128.
(64) Minor, E. C.; Swenson, M. M.; Mattson, B. M.; Oyler, A. R. *Environ. Sci. Process. Impacts* **2014**, *16* (9), 2064−2079.
(65) McLafferty, F. W.; Turecek, F. *Interpretation of Mass Spectra*; University Science Books: Mill Valley, CA, 1993; p 371.
(66) Boye, K.; Noël, V.; Tfaily, M. M.; Bone, S. E.; Williams, K. H.; Bargar, J. R. R.; Fendorf, S. *Nat. Geosci.* **2017**, *10* (6), 415−419.

https://doi.org/10.1021/acs.analchem.2c02377
Anal. Chem. 2022, 94, 11382−11389